

## Fitting-free construction of nonlocal resonance models for nuclear dynamics of electron-molecule collisions

Václav Alt<sup>ⓧ,\*</sup>, Martin Čížek<sup>ⓧ,†</sup> and Karel Houfek<sup>ⓧ,‡</sup>

*Institute of Theoretical Physics, Faculty of Mathematics and Physics, Charles University, V Holešovičkách 2, 180 00 Praha 8, Czech Republic*

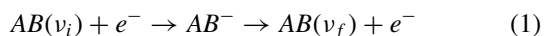
 (Received 9 November 2023; accepted 22 April 2024; published 15 May 2024)

The nonlocal resonance models for nuclear dynamics of low-energy electron-molecule collisions are usually constructed by fitting necessary quantities to the potential energy curves (surfaces) and the eigenphase sums obtained from fixed-nuclei quantum chemistry and scattering calculations. Moreover, the fitting functions have to be chosen in such a way to be able to evaluate the Hilbert transform, which appears in the nonlocal potential, in a closed form. This procedure can be rather elaborate for polyatomic molecules when more than one degree of freedom for nuclear motion is considered. In this paper we propose an alternative, fitting-free way of constructing these models directly from the fixed-nuclei level-shift function that is completely determined by the choice of the discrete state defining the nonlocal resonance model. The Hilbert transform is evaluated numerically using the fast Fourier transform. Using the numerically solvable two-dimensional model of resonant electron-molecule collisions, we demonstrate that the results of nonlocal models constructed using the proposed approach agree with the exact ones up to contributions from background scattering, which can often be neglected for inelastic processes. For completeness, we also compare the results of the proposed method with the usual fitting approach, showing that the proposed fitting-free method of construction of the nonlocal resonance models is more reliable and accurate.

DOI: [10.1103/PhysRevA.109.052817](https://doi.org/10.1103/PhysRevA.109.052817)

### I. INTRODUCTION

In low-energy collisions of electrons with molecules, the electron is often captured by the molecule into a quasi-bound-state, resulting in the efficient energy transfer between electronic and nuclear motion [1,2], leading to, e.g., inelastic processes of vibrational excitation of the molecule



and dissociative electron attachment



where  $A$  and  $B$  stand for either atoms in diatomic molecules or suitable parts of a polyatomic molecule. As a proper treatment of nuclear dynamics plays an important role in these processes, their theoretical description is usually based on the construction of an effective model for nuclear dynamics based on the data from the fixed-nuclei electron-scattering calculations [2,3]. Several approaches for treating the nuclear dynamics have been proposed, e.g., the local complex potential approximation [4,5] or the  $R$ -matrix method [6]. Here we mainly discuss the nonlocal resonance model (NRM), which is more rigorous than the local approach [7,8] and is based on the projection-operator formalism [5], originally developed for nuclear reactions by Feshbach [9,10] and later

adapted to electron-molecule collisions [11–15]. The nonlocal theory is necessary to properly describe processes where threshold effects play an important role [5,16]. It has been applied to many diatomic molecules [5,17] and also to polyatomic molecules considering only some vibrational degrees of freedom [18–20,22]. Although recently the full vibrational dynamics of the  $\text{CO}_2$  molecule has been treated with this approach [23–25], the resulting model fitted to the *ab initio* data is rather complicated, and a new fitting-free approach to construct such models would be quite advantageous.

The nonlocal theory is based on a suitable choice of one or more discrete states and the corresponding separation of the electronic Hilbert space into the discrete-state (resonant) and background part. The nuclear dynamics is then solved after projection onto the discrete-state part to obtain the cross sections for the processes (1) and (2). However, the nonlocal models have been directly constructed using an explicitly chosen discrete state only in a few cases [26–28] because of the difficulties with the construction of the background part of the electronic basis and numerical evaluation of the nonlocal potential via the Hilbert transform which appears in the effective equation describing the nuclear dynamics. Berman *et al.* [26] calculated the discrete-state energy, resonance width, and level-shift function from the first principles for the  $^2\Sigma_u^+$  resonance in electron-molecule scattering and then fitted these functions to obtain the discrete-state–continuum coupling as a suitable function of energy and internuclear distance which enabled them to treat the Hilbert transform exactly [27]. Houfek *et al.* [29] proposed a simple two-dimensional model of electron-molecule collisions for testing various approximations used to treat the nuclear dynamics of these collisions

\*vaclav.alt@utf.mff.cuni.cz

†Martin.Cizek@mff.cuni.cz

‡Karel.Houfek@mff.cuni.cz

and constructed the nonlocal model starting with a discrete state and evaluating all necessary quantities, including background contributions, numerically [28]. Unfortunately, this direct approach is quite difficult to use for many-electron molecules. Therefore, the nonlocal models have usually been constructed by fitting the potential energy curves (surfaces) and the eigenphase sums obtained from fixed-nuclei quantum chemistry and scattering calculations. The model functions are often chosen in such a way as to evaluate the Hilbert transform, which appears in the nonlocal potential, in a closed form (see [5] and references therein).

Here we propose an alternative, fitting-free way of constructing the nonlocal models directly from *ab initio* electron-scattering calculations without the need to find the background scattering states. Such models do not allow the evaluation of the Hilbert transform in the nonlocal potential in a closed form, but we show how it can be evaluated numerically using the fast Fourier transform. We demonstrate the applicability of this approach within the two-dimensional models for three diatomic molecules and compare it with constructing the nonlocal models based on the fitting of phase shifts or eigenphase sums.

## II. THEORY

It is difficult to obtain the converged numerical results for real molecules even in the case of the smallest neutral molecule  $H_2$  [26,30]. To compare various methods of construction of the NRM, we use instead a simple two-dimensional toy model of the electron-molecule interactions [29], which can be solved exactly numerically without any approximations that are necessary for real systems. Note that it is only a toy model, not aimed at a comparison with the experiment. However, it can be used to probe various approximations of the resonant nuclear dynamics in electron-molecule collisions. In this section we briefly introduce this two-dimensional model and the key concepts of the nonlocal discrete-state-in-continuum theory. We also discuss the numerical evaluation of the Hilbert transform.

### A. Two-dimensional model

The Hamiltonian of the two-dimensional model is given by

$$H = T_R + T_r + V(R, r), \quad (3)$$

$$V(R, r) = V_0(R) + \frac{l(l+1)}{2r^2} + V_{\text{int}}(R, r), \quad (4)$$

where

$$T_R = -\frac{1}{2\mu} \frac{\partial^2}{\partial R^2}, \quad T_r = -\frac{1}{2} \frac{\partial^2}{\partial r^2} \quad (5)$$

are nuclear and electronic kinetic energy operators, with  $\mu$  the reduced mass of the nuclei of the modeled diatomic molecule. Potential energy  $V_0(R)$  drives the vibrational motion of the neutral molecule and the other two terms in (4) reproduce the resonant behavior of the molecular negative ion.

A detailed formulation of the dynamics of collision processes (1) and (2) within this model, its numerical solution, and calculation of the cross sections for two specific models for molecules  $N_2$  and  $NO$  can be found in [29]. Both potentials

TABLE I. Parameters of the two-dimensional models [29]. All values are in atomic units.

Parameter	$N_2$	$NO$
$\mu$	12766.36	13614.16
$l$	2 ( <i>d</i> wave)	1 ( <i>p</i> wave)
$D_0$	0.75102	0.2363
$\alpha_0$	1.15350	1.571
$R_0$	2.01943	2.157
$\lambda_\infty$	6.21066	6.367
$\lambda_1$	1.05708	5.0
$R_\lambda$	-27.9833	2.0843
$\lambda_c$	5.38022	6.05
$R_c$	2.405	2.285
$\alpha_c$	0.4	1.0

$V_0(R)$  and  $V_{\text{int}}(R, r)$  for these two models are of the same form

$$V_0(R) = D_0(e^{-2\alpha_0(R-R_0)} - 2e^{-\alpha_0(R-R_0)}), \quad (6)$$

$$V_{\text{int}}(R, r) = -\lambda(R)e^{-\alpha_c r^2}, \quad (7)$$

where  $\lambda(R)$  is given by

$$\lambda(R) = \lambda_\infty + \frac{\lambda_0}{1 + e^{\lambda_1(R-R_\lambda)}}, \quad (8)$$

$$\lambda_0 = (\lambda_c - \lambda_\infty)(1 + e^{\lambda_1(R_c-R_\lambda)}). \quad (9)$$

All parameters for the  $N_2$  and  $NO$  models are summarized in Table I.

The potentials of the third model for the  $O_2$  molecule differ from the previous two because the simple functions used for  $N_2$ -like and  $NO$ -like models are not suitable to imitate the potential energy curves of the real  $O_2$  system as obtained, for example, in [31]. The neutral potential energy  $V_0(R)$  is composed of two parts:  $V_{\text{well}}(R)$  describing the well in the vicinity of the energy minimum around  $R_0$  and  $V_{\text{lr}}(R)$  describing the long-range behavior. The switching functions  $\theta_i(R)$  enable a smooth transition between the two terms:

$$\begin{aligned} V_0(R) &= V_{\text{well}}(R)\theta_1(R) + V_{\text{lr}}(R)\theta_2(R), \\ V_{\text{well}}(R) &= -D_0(1 + \alpha\xi + \beta_1\xi^2 + \beta_2\xi^3)e^{-\alpha\xi}, \\ \xi &= R - R_0, \\ V_{\text{lr}}(R) &= \frac{\omega_1}{R^4} + \frac{\omega_2}{R^6}, \\ \theta_i(R) &= \frac{1}{2}\{1 - \tanh[a_i(\xi_i + e^{b_i\xi_i} - 1)]\}, \\ \xi_i &= (-1)^{c_i}(R - R_{i0}). \end{aligned} \quad (10)$$

Although the parameters of these functions are determined by a least-squares fit to the *ab initio* data obtained in [31], we should note that it is not important how well they reproduce the potential energy curves of the real system as the two-dimensional model is considered to be only a toy model, not determined for direct comparison with experiment. The values of all  $O_2$ -like model parameters are listed in Table II to the precision needed to reproduce our results. The interaction

TABLE II. Parameters of the O<sub>2</sub> neutral potential energy curve. All values are in atomic units.

Parameter	Value	Parameter	Value
$D_0$	0.23178	$R_{10}$	4.25451
$\alpha$	1.96203	$a_1$	0.589844
$R_0$	2.29989	$b_1$	3.19454
$\beta_1$	-0.197253	$c_1$	0.0
$\beta_2$	-0.453587	$R_{20}$	2.632224
$\omega_1$	-1.263645	$a_2$	0.270386
$\omega_2$	28.9218	$b_2$	2.55552
		$c_2$	1.0

potential differs in the choice of the function  $\lambda(R)$ ,

$$\lambda(R) = \lambda_\infty + \sum_{i=1}^2 \frac{\lambda_{0i}}{1 + e^{\lambda_{1i}(R-R_{1i})}}, \quad (11)$$

the parameters of which are in Table III. The resulting two-dimensional potential for the O<sub>2</sub>-like model is shown in Fig. 1.

### B. Discrete-state-in-continuum theory and nonlocal resonance models

The discrete-state-in-continuum theory [5,9,10], on which the construction of nonlocal resonance models is based, is a framework for studying nuclear dynamics in collision processes like (1) and (2). For simplicity, we formulate the theory only for the two-dimensional (2D) model described above; for a more general discussion of application to negative molecular ions see, for example, [5,32].

Within the discrete-state-in-continuum approach, it is assumed that the incident electron gets trapped in a discrete (often resonant) state  $|\phi_d\rangle$ , forming a metastable molecular anion. The description of the dynamics is based on the Feshbach projection-operator approach [9,10], the main idea of which lies in the separation of the electronic Hilbert space into the resonant and the background parts, using the projection operators defined by the discrete state

$$Q = |\phi_d\rangle \langle \phi_d|, \quad (12)$$

$$P = \mathbb{1} - Q. \quad (13)$$

In the background part of the electronic Hilbert space, we can take as a basis the outgoing background scattering states  $\phi_\varepsilon$  which are orthogonal to the discrete state and solve the

TABLE III. Parameters of the O<sub>2</sub>-like two-dimensional model. All values are in atomic units.

Parameter	Value	Parameter	Value
$\mu$	14682.6	$l$	2 ( $d$ wave)
$\lambda_\infty$	1.9792	$\alpha_c$	0.133
$\lambda_{01}$	-38.9401	$\lambda_{02}$	0.230156
$\lambda_{11}$	1.63986	$\lambda_{12}$	1.4806
$R_{\lambda 1}$	-0.448295	$R_{\lambda 2}$	4.46478

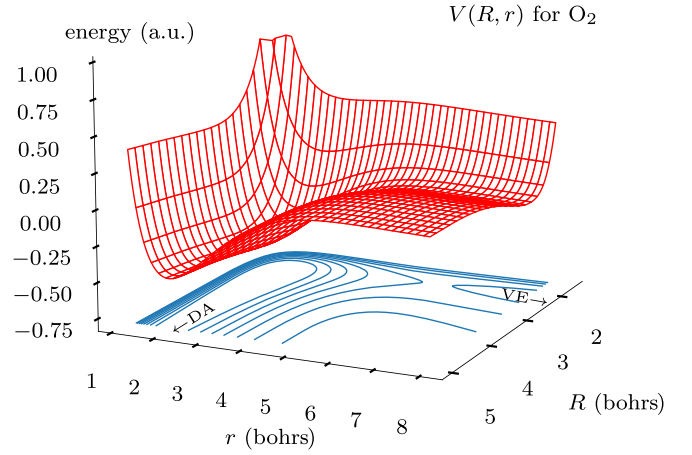


FIG. 1. Two-dimensional potential of the O<sub>2</sub>-like model.

equation

$$PH_{\text{el}}P|\phi_\varepsilon\rangle = [V_0(R) + \varepsilon]|\phi_\varepsilon\rangle, \quad (14)$$

where  $H_{\text{el}}$  is the electronic Hamiltonian, defined within the two-dimensional model as

$$H_{\text{el}} = T_r + V(R, r). \quad (15)$$

Once a suitable discrete state  $|\phi_d\rangle$  is chosen (see [28] for a detailed discussion) we can define the matrix elements of the electronic Hamiltonian

$$V_d(R) = \langle \phi_d | H_{\text{el}} | \phi_d \rangle, \quad (16)$$

$$V_{d\varepsilon}(R) = \langle \phi_d | H_{\text{el}} | \phi_\varepsilon \rangle, \quad (17)$$

which are, together with the neutral molecule potential energy function  $V_0(R)$ , the main building blocks of nonlocal resonance models.

In the electron-molecule collision processes, the initial vibrational state  $\eta_{v_i}(R)$  with energy  $E_{v_i}$  is given by

$$[T_R + V_0(R)]\eta_{v_i}(R) = E_{v_i}\eta_{v_i}(R). \quad (18)$$

The electron arriving with energy  $\varepsilon_i$  yields the total energy  $E = E_{v_i} + \varepsilon_i$ . The nuclear wave function  $\Psi_d(R)$  corresponding to the discrete-state part of the Hilbert space can be obtained by solving the equation [28]

$$\begin{aligned} [E - T_R - V_d(R)]\Psi_d(R) - \int dR' F(E, R, R')\Psi_d(R') \\ = V_{d\varepsilon_i}(R)\eta_{v_i}(R). \end{aligned} \quad (19)$$

The interaction with the electronic continuum is effectively described by the complex, nonlocal, and energy-dependent potential

$$F(E, R, R') = \int d\varepsilon' \frac{V_{d\varepsilon'}(R)V_{d\varepsilon'}^*(R')}{E - T_R - V_0 - \varepsilon' + i\eta}. \quad (20)$$

For a practical evaluation, it is useful to expand the Green's function in  $F(E, R, R')$  into the vibrational states  $\eta_v(R)$  of the

neutral molecule given by (18). This expansion can be written as

$$\begin{aligned} F(E, R, R') &= \sum_v \eta_v(R) \tilde{F}(\varepsilon_v, R, R') \eta_v^*(R') \\ &= \sum_v \eta_v(R) \left( \tilde{\Delta}(\varepsilon_v, R, R') \right. \\ &\quad \left. - \frac{i}{2} \tilde{\Gamma}(\varepsilon_v, R, R') \right) \eta_v^*(R'), \end{aligned} \quad (21)$$

where  $\varepsilon_v = E - E_v$  is the virtual electron energy corresponding to the molecule in the vibrational state  $\eta_v(R)$ .

From Eqs. (20) and (21) we can see that

$$\tilde{F}(\varepsilon, R, R') = \int d\varepsilon' \frac{V_{d\varepsilon'}(R) V_{d\varepsilon'}^*(R')}{\varepsilon - \varepsilon' + i\eta}, \quad (22)$$

which can be further rewritten with the Cauchy principal value

$$\tilde{F}(\varepsilon, R, R') = \text{P.V.} \int d\varepsilon' \frac{\gamma(\varepsilon', R, R')}{\varepsilon - \varepsilon'} - i\pi \gamma(\varepsilon, R, R'), \quad (23)$$

where we also introduced the following notation for simplification:

$$\gamma(\varepsilon, R, R') = 2\pi V_{d\varepsilon}(R) V_{d\varepsilon}^*(R'). \quad (24)$$

For the actual calculations, the real and imaginary parts of  $\tilde{F}(\varepsilon, R, R')$  for complex  $V_{d\varepsilon}(R)$  can be expressed as

$$\begin{aligned} \tilde{\Delta}(\varepsilon, R, R') &= \text{Re}[\tilde{F}(\varepsilon, R, R')] \\ &= \frac{1}{2\pi} \text{P.V.} \int d\varepsilon' \frac{\text{Re}[\gamma(\varepsilon', R, R')]}{\varepsilon - \varepsilon'} \\ &\quad + \frac{1}{2} \text{Im}[\gamma(\varepsilon, R, R')] \end{aligned} \quad (25)$$

and

$$\begin{aligned} \tilde{\Gamma}(\varepsilon, R, R') &= -2i \text{Im}[\tilde{F}(\varepsilon, R, R')] \\ &= \text{Re}[\gamma(\varepsilon, R, R')] \\ &\quad - \frac{1}{\pi} \text{P.V.} \int d\varepsilon' \frac{\text{Im}[\gamma(\varepsilon', R, R')]}{\varepsilon - \varepsilon'}, \end{aligned} \quad (26)$$

where P.V. denotes the Cauchy principal value. If  $\gamma(\varepsilon, R, R')$  is real, the functions  $\tilde{\Delta}(\varepsilon, R, R')$  and  $\tilde{\Gamma}(\varepsilon, R, R')$  reduce to the usual, simpler form

$$\tilde{\Delta}(\varepsilon, R, R') = \frac{1}{2\pi} \text{P.V.} \int d\varepsilon' \frac{\tilde{\Gamma}(\varepsilon', R, R')}{\varepsilon - \varepsilon'}, \quad (27)$$

$$\tilde{\Gamma}(\varepsilon, R, R') = 2\pi V_{d\varepsilon}(R) V_{d\varepsilon}^*(R'). \quad (28)$$

Once Eq. (19) is solved for the discrete-state part  $\Psi_d(R)$  of the nuclear wave function, we can determine the contribution corresponding to the cross sections for processes (1) and (2) using

$$\sigma_{v_i v_f}(\varepsilon) = \frac{4\pi^3}{k_i^2} |\langle \eta_{v_f} | V_{d\varepsilon_f} | \Psi_d \rangle|^2, \quad (29)$$

$$\sigma_{\text{DA}} = \frac{2\pi^2 K}{k_i^2} \lim_{\mu \rightarrow \infty} |\Psi_d(R)|^2, \quad (30)$$

where  $k_i = \sqrt{2\varepsilon_i}$  is the momentum corresponding to energy  $\varepsilon_i$  of the incoming electron,  $\varepsilon_f$  is the energy of the outgoing

electron, and  $K$  is the relative momentum of the outgoing nuclei in the dissociative attachment (DA) channel with energy  $E - V_d(R)|_{R \rightarrow \infty} = K^2/2\mu$ .

### C. Numerical evaluation of the Hilbert transform

The Hilbert transform in Eqs. (25)–(27) is usually evaluated in a closed form if  $V_{d\varepsilon}(R)$  or  $\Gamma(\varepsilon, R)$  are chosen to be of a suitable form, as in Eq. (46), when a fitting procedure is used to construct the nonlocal model. However, in a simple form, the analytic ansatz may be too restrictive to obtain a reasonable fit, and adding too many terms leads to ambiguities and makes the fitting procedure very tedious, especially in the attempts to generalize the approach to larger molecules.

One can alternatively evaluate the Hilbert transform directly using the Fourier transform, exploiting a simple relation between these two transforms. For its derivation, we use the definitions of the Fourier transform and its inverse

$$\mathcal{F}[f](t) = \int_{-\infty}^{\infty} f(\varepsilon) e^{-i\varepsilon t} d\varepsilon, \quad (31)$$

$$\mathcal{F}^{-1}[f](\varepsilon) = \frac{1}{2\pi} \int_{-\infty}^{\infty} f(t) e^{i\varepsilon t} dt \quad (32)$$

and of the Hilbert transform

$$\mathcal{H}[f](\varepsilon) = \frac{1}{\pi} \text{P.V.} \int_{-\infty}^{\infty} \frac{f(\varepsilon')}{\varepsilon - \varepsilon'} d\varepsilon' = \frac{1}{\pi} [g * f](\varepsilon), \quad (33)$$

where  $g * f$  denotes the convolution of the function  $g(\varepsilon) = 1/\varepsilon$  with  $f(\varepsilon)$ . Applying the Fourier transform to the Hilbert transform of the function  $f(\varepsilon)$  and using the convolution theorem yields

$$\mathcal{F}[\mathcal{H}[f]](t) = (-i \text{sgn} t) \mathcal{F}[f](t) = h(t) \quad (34)$$

since the Fourier transform (given as a principal value integral) of the function  $g(\varepsilon)$  is given by the signum function as  $-i\pi \text{sgn} t$ . By taking the inverse Fourier transform of the function  $h(t)$ , we finally get

$$\mathcal{H}[f](\varepsilon) = \mathcal{F}^{-1}[h](\varepsilon). \quad (35)$$

This rather simplified derivation provides a particularly valuable way of evaluating the Hilbert transform that is commonly used for its numerical evaluation using the fast Fourier transform. A more detailed discussion can be found in [33] and references therein.

Using Eqs. (34) and (35), the function  $\tilde{\Delta}(\varepsilon, R, R')$ , given as a Hilbert transform in (27) up to the factor  $\frac{1}{2}$ , can be evaluated applying the Fourier transform only. For each internuclear distance  $R$  and  $R'$ , we calculate first the function

$$\tilde{h}(t) = -i \text{sgn} t \int_{-\infty}^{\infty} \tilde{\Gamma}(\varepsilon, R, R') e^{-i\varepsilon t} d\varepsilon, \quad (36)$$

where  $\tilde{\Gamma}(\varepsilon, R, R') = 0$  for  $\varepsilon < 0$ , and then  $\tilde{\Delta}(\varepsilon, R, R')$  is given by the inverse Fourier transform

$$\tilde{\Delta}(\varepsilon, R, R') = \frac{1}{2} \mathcal{F}^{-1}[\tilde{h}](\varepsilon) = \frac{1}{4\pi} \int_{-\infty}^{\infty} \tilde{h}(t) e^{i\varepsilon t} dt. \quad (37)$$

For simplicity, we restricted the example to real  $V_{d\varepsilon}(R)$ . Application to the general case of complex  $V_{d\varepsilon}(R)$  in Eqs. (25) and (26) is straightforward.

### III. CONSTRUCTION OF NONLOCAL RESONANCE MODELS

In this section we define two kinds of discrete state  $\phi_d$  that we use to construct the nonlocal resonance models. Then we formulate the proposed method of obtaining the discrete-state-continuum coupling from an *ab initio* level-shift function. Finally, we summarize the usual process of NRM construction by fitting, as we compare it later with the method introduced herein.

#### A. Choice of discrete state

To construct nonlocal models in an *ab initio* way, one has to choose the discrete state  $\phi_d$ . When the validity of the nonlocal approach was tested within the 2D model, several different discrete states  $\phi_d$  were discussed in [28]. Here we use two of those discrete states that sufficiently illustrate various constructions of the nonlocal models.

The first choice is a constant discrete state independent of the internuclear distance. It is chosen as the electronic bound state in the limit  $R \rightarrow \infty$ , i.e., the solution of the equation

$$\left(T_r + \frac{l(l+1)}{2r^2} + V_b(r)\right)\phi_d^{\text{const}}(r) = -E_{\text{EA}}\phi_d^{\text{const}}(r), \quad (38)$$

where the potential

$$V_b(r) = \lim_{R \rightarrow \infty} V_{\text{int}}(R, r) \quad (39)$$

supports one electronic bound state and  $E_{\text{EA}}$  is the electron affinity of the atomic anion. This will be referred to as the constant choice of the discrete state.

The second choice is a discrete state chosen as the lowest-lying bound state of a modified electronic Hamiltonian (15) where the function  $\lambda(R)$  is changed in such a way that the resulting potential supports one bound electronic state for all internuclear distances. Thus the discrete state in this case is the solution of the equation

$$\left(T_r + \frac{l(l+1)}{2r^2} - \lambda_{\text{spec}}(R)e^{-\alpha r^2}\right)\phi_d^{\text{spec}}(r) = E\phi_d^{\text{spec}}(r), \quad (40)$$

where the function  $\lambda_{\text{spec}}(R)$  takes the form

$$\lambda_{\text{spec}}(R) = \lambda_{\infty} + \frac{\lambda_{-\infty} - \lambda_{\infty}}{1 + e^{c_d(R-R_d)}}. \quad (41)$$

Such a discrete state will be identified by the choice of parameters  $\lambda_{-\infty}$ ,  $c_d$ , and  $R_d$ . In contrast to the constant choice, this discrete state is more compact and smoothly varying with  $R$ . This will be referred to as the special choice of the discrete state.

#### B. Construction from the *ab initio* level shift

Direct *ab initio* evaluation of the coupling elements  $V_{d\varepsilon}(R)$  defined by (17) is difficult because of the necessity of finding the background scattering states (14) orthogonal to the discrete state  $\phi_d$ . Therefore, the determination of  $V_{d\varepsilon}(R)$  for real systems has usually been based on fitting the eigenphase sums obtained from the fixed-nuclei electron scattering calculations as described in the next section. If a nonlocal model is not built directly from a specific discrete state  $\phi_d$ , the background contribution is not uniquely determined and its energy dependence during the fitting procedure has to be assumed. To avoid

this ambiguity, we propose to determine the coupling  $V_{d\varepsilon}(R)$  from the complex energy-dependent function

$$F(\varepsilon, R) = \Delta(\varepsilon, R) - \frac{i}{2}\Gamma(\varepsilon, R), \quad (42)$$

which is the fixed-nuclei counterpart of the nonlocal potential  $F(E, R, R')$  and can be obtained in the following way.

When solving the fixed-nuclei electron scattering, we can express the electronic Hamiltonian in the basis consisting of the discrete state  $\phi_d$  and the complementary background scattering states  $\phi_\varepsilon$  as the matrix

$$H_{\text{el}} = \begin{pmatrix} V_d(R) & \cdots & V_{d\varepsilon}(R) & \cdots \\ \vdots & \ddots & \vdots & \vdots \\ V_{d\varepsilon}^*(R) & & V_0(R) + \varepsilon & \\ \vdots & & & \ddots \end{pmatrix}.$$

The discrete-state matrix element of the corresponding Green's function  $G^+(\varepsilon) = (\varepsilon - H_{\text{el}} + i\eta)^{-1}$  is then given by the Schur complement [34], i.e.,

$$\langle \phi_d | G^+(\varepsilon) | \phi_d \rangle = [\varepsilon - V_d(R) - F(\varepsilon, R)]^{-1}, \quad (43)$$

where

$$F(\varepsilon, R) = \int d\varepsilon' \frac{V_{d\varepsilon'}(R)V_{d\varepsilon'}^*(R)}{E - V_0(R) - \varepsilon' + i\eta}.$$

Expressing  $F(\varepsilon, R)$  from (43), we get

$$F(\varepsilon, R) = \varepsilon - V_d(R) - \frac{1}{\langle \phi_d | G^+(\varepsilon) | \phi_d \rangle}. \quad (44)$$

Thus, if one could somehow calculate the matrix element  $\langle \phi_d | G^+(\varepsilon) | \phi_d \rangle$ , the resonance-width function  $\Gamma(\varepsilon, R)$ , given up to a factor as the imaginary part of  $F(\varepsilon, R)$  in (42), can

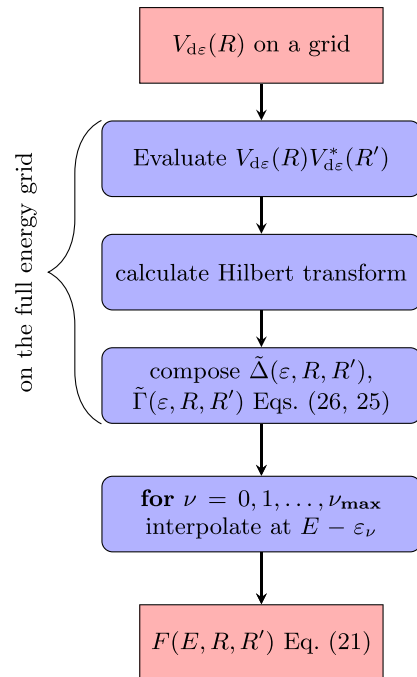


FIG. 2. Structure of the  $F(E, R, R')$  evaluation from  $V_{d\varepsilon}(R)$  pre-calculated on an  $\varepsilon$ - $R$  grid.

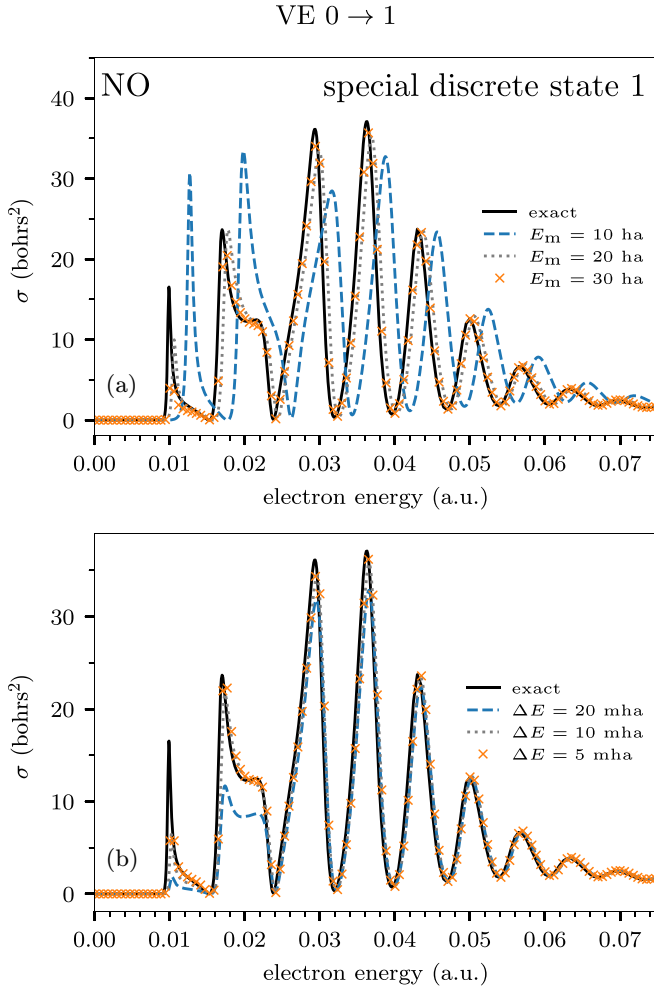


FIG. 3. Convergence of the cross sections with (a) the integration range  $E_m$  and (b) the energy discretization step  $\Delta E$  of the Hilbert transform grid. Results for the spec1 discrete state are compared with the exact results calculated from the NO-like two-dimensional model, using (a)  $\Delta E = 10$  mhartree and (b)  $E_m = 30$  hartree.

be used to determine the discrete-state-continuum coupling  $V_{d\varepsilon}(R)$  [compare with (28)] as

$$V_{d\varepsilon}(R) = \sqrt{\frac{\Gamma(\varepsilon, R)}{2\pi}}. \quad (45)$$

In contrast to the original definition (17),  $V_{d\varepsilon}(R)$  given by (45) is always real, thus losing some information about the relative phase between  $V_{d\varepsilon}(R)$  and  $V_{d\varepsilon}(R')$  that could be important in (20). In models of real systems, it is usually assumed that this relative phase can be neglected [32]. As shown below, in all our studied model cases, its influence on the results seems to be insignificant.

Although the evaluation of  $\langle \phi_d | G^+(\varepsilon) | \phi_d \rangle$  can be nontrivial in real many-electron systems, it is in principle possible, for example, in the  $R$ -matrix approach where the Green's function  $G^+(\varepsilon)$  can be expressed using the  $R$ -matrix energies and states. Thus, in this way, the determination of the background electronic states  $\phi_\varepsilon$  can be avoided completely.

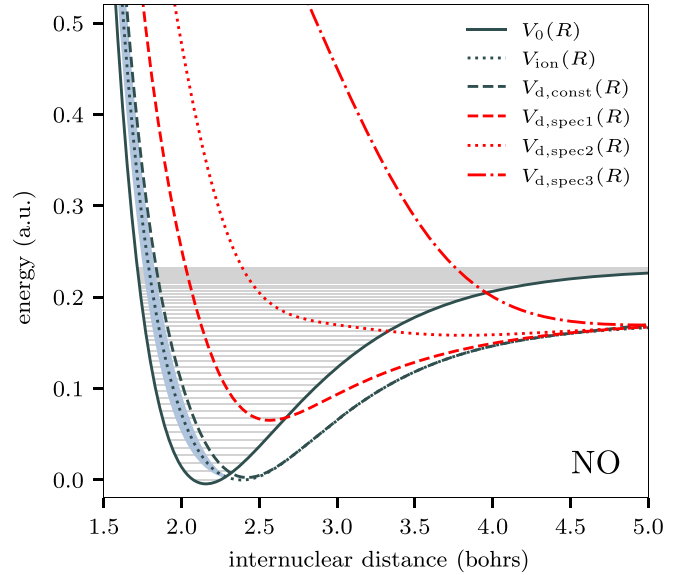


FIG. 4. Potential energy curves of the NO-like model: the neutral potential  $V_0(R)$ , the negative ion resonance  $V_{\text{ion}}(R)$ , and the resonance width (shown by the shaded area) together with the discrete-state potentials  $V_d(R)$  for the constant and three special choices of the discrete state.

### C. Construction by fitting

For completeness, we describe here also a usual way of constructing the nonlocal resonance models by fitting. During this procedure, the functions  $V_0(R)$ ,  $V_d(R)$ , and  $V_{d\varepsilon}(R)$  are assumed to have a certain dependence on internuclear distance and energy with several unknown parameters.

The neutral potential  $V_0(R)$  usually comes from quantum chemistry calculations and is either interpolated or fitted with a suitable function. Here we use the potential  $V_0(R)$  as it is defined within the two-dimensional models.

A common choice [8] of the functional form of  $V_{d\varepsilon}(R)$  is

$$V_{d\varepsilon}(R) = \varepsilon^{\alpha/2} \sum_{i=1}^n A_i(R) e^{-B_i(R)\varepsilon}, \quad (46)$$

with  $\alpha = l + \frac{1}{2}$ , for which one can evaluate the Hilbert transform in Eq. (27) in a closed form [7]. The functions  $A_i(R)$  and  $B_i(R)$  are usually determined by fitting the eigenphase sums obtained from fixed-nuclei electron scattering calculations by the generalized Breit-Wigner formula

$$\delta(\varepsilon, R) = -\arctan\left(\frac{\tilde{\Gamma}(\varepsilon, R)/2}{E - V_d(R) - \tilde{\Delta}(\varepsilon, R) + V_0(R)}\right) + \delta_{\text{bg}}(\varepsilon, R). \quad (47)$$

For simplicity, we take the background contribution to the eigenphase sums in a simple linear form

$$\delta_{\text{bg}}(\varepsilon, R) = a(R)\varepsilon + b(R).$$

The discrete-state potential  $V_d(R)$  that enters the formula (47) can be fitted together with functions  $A_i(R)$  and  $B_i(R)$  assuming, for example, the Morse potential form and ensuring

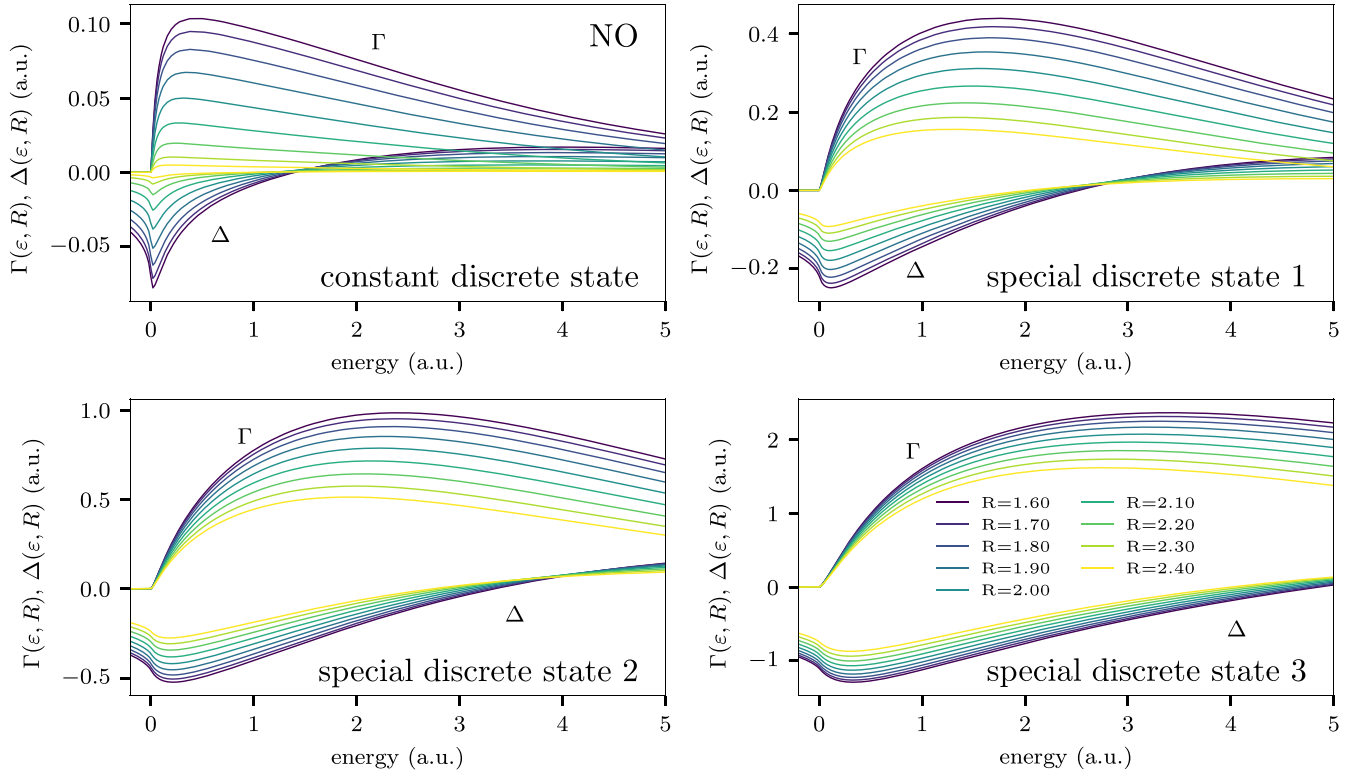


FIG. 5. Fixed-nuclei level-shift functions  $\Delta(\varepsilon, R)$  and resonance widths  $\Gamma(\varepsilon, R)$  for all choices of the discrete state for NO.

the proper asymptotic behavior

$$V_d(R) \xrightarrow{R \rightarrow \infty} V_{\text{ion}}(R)$$

for large internuclear distances  $R$  where it corresponds to the bound anion state. If there is a clear resonance in the system, one can alternatively use the resonance energy  $E_{\text{res}}(R)$ , if it is known from fixed-nuclei scattering calculations, to determine the discrete-state potential directly using the relation

$$V_d(R) = V_0(R) + E_{\text{res}}(R) - \Delta(E_{\text{res}}(R), R). \quad (48)$$

#### IV. CALCULATIONS AND RESULTS

We use three two-dimensional ( $\text{N}_2$ -like, NO-like, and  $\text{O}_2$ -like) models to compare three ways of NRM construction. One way is to directly calculate the discrete-state–continuum coupling  $V_{d\varepsilon}(R)$  from the background scattering states using the definition (17) and all other quantities to verify the viability of the numerical evaluation of the Hilbert transform. The second way is to determine the *ab initio* level-shift function  $F(\varepsilon, R)$  from the formula (44) to test the proposed method. The third way is to calculate the fixed-nuclei scattering phase shifts  $\delta(\varepsilon, R)$  to serve as the input data that can be fitted by (47), which is the method that has been mostly used in the calculations for real systems.

In our calculations, the functions  $V_{d\varepsilon}(R)$  and  $F(\varepsilon, R)$  are precalculated on an energy and internuclear distance grid. The properties of this grid have to be chosen properly to achieve the convergence of the resulting cross sections, as discussed below.

The direct calculation of  $V_{d\varepsilon}(R)$  consists of finding the background scattering states defined in Eq. (14) and direct

evaluation of the matrix elements in Eq. (17). The details are described in [28].

The fixed-nuclei level-shift function  $F(\varepsilon, R)$  is calculated directly from Eq. (44). For the given discrete state  $\phi_d(r; R)$ , the matrix element  $\langle \phi_d | G^+(\varepsilon) | \phi_d \rangle$  is calculated by projecting the discrete state to  $|\xi\rangle$ , computed as the solution of the Schrödinger equation

$$(\varepsilon - H_{\text{el}}) |\xi\rangle = |\phi_d\rangle \quad (49)$$

that is solved by employing the numerical grid method with exterior complex scaling ensuring the outgoing boundary conditions as introduced in [35]. The discrete-state potential  $V_d(R)$  is calculated from Eq. (16).

In the expansion in Eq. (21),  $\tilde{F}(\varepsilon_v, R, R')$  is evaluated at energies given by  $\varepsilon_v = E - E_v$  which do not generally coincide with the energy grid suitable for the fast Fourier transform on which  $V_{d\varepsilon}(R)$  is precalculated. For this reason, the values of  $\tilde{F}(\varepsilon_v, R, R')$  must be interpolated in energy. The procedure of the full  $F(E, R, R')$  evaluation is outlined in Fig. 2.

These calculations were performed for each model for a constant discrete state and one or more special discrete states.

##### A. Convergence of the evaluation of the Hilbert transform

Before we compare results for nonlocal resonance models constructed in different ways, we briefly discuss the convergence of the proposed method of evaluation of the Hilbert transform using the fast Fourier transform. We limit the discussion to only the NO-like model. The results are similar for other models and we show them in the Supplemental Material [36].

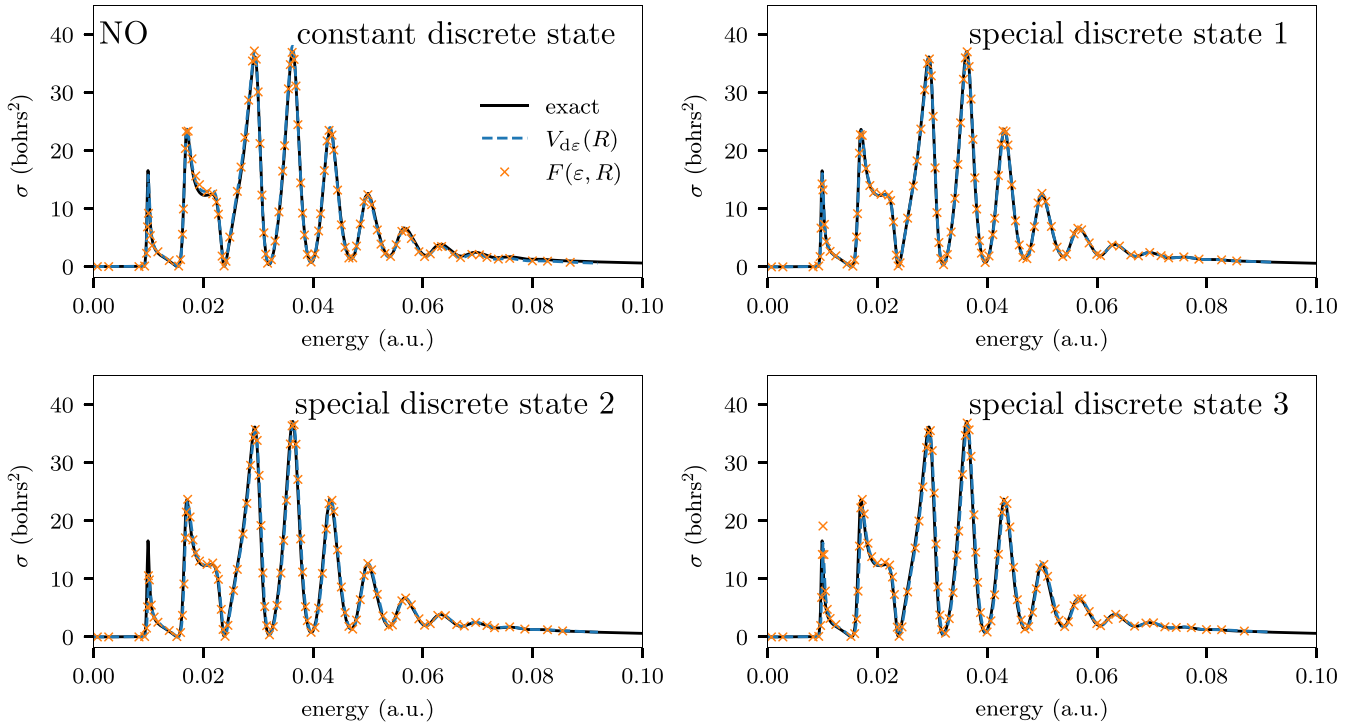
VE  $0 \rightarrow 1$ 

FIG. 6. Vibrational excitation cross section for all choices of the discrete state for NO.

For the constant discrete state, the discrete-state-continuum coupling  $V_{d\epsilon}(R)$  is relatively compact in energy [compare the resonance width functions  $\Gamma(\epsilon, R)$  in Fig. 5 shown for different discrete states below] and integration up to 10 a.u. proved sufficient to achieve convergence. In the case of the special discrete states as  $\lambda_{-\infty}$  increases,  $\phi_d$  becomes more and more compact while its energy  $V_d(R)$  increases. Because of that,  $V_{d\epsilon}(R)$  decays slowly in energy and one needs to integrate to high energies to get accurate  $\Delta(\epsilon, R)$ . For example, to achieve convergence for the special discrete state defined by the parameters  $\lambda_{-\infty} = 8$ ,  $c = 1.8$ , and  $R_d = 3.0$ , it is necessary to integrate up to 30 a.u. Otherwise, the  $\Delta(\epsilon, R)$  function is too small, resulting in the wrong positions of the peaks in the vibrational excitation cross section, as can be observed in Fig. 3(a). For the most compact discrete state used here for the NO-like model with  $\lambda_{-\infty} = 15$ , it is necessary to integrate even up to 200 a.u. Such large integration ranges can be a problem in the calculations for real systems, as direct evaluation of  $V_{d\epsilon}(R)$  or  $F(\epsilon, R)$  to such energies may be difficult and impractical. However, one can circumvent this, for example, by splitting  $\Gamma(\epsilon, R)$  into two terms: the long-range envelope, the Hilbert transform of which is known [such as in Eq. (46)], and the short-range deviation, the Hilbert transform of which can be calculated numerically, supposedly on a much smaller energy range.

Because of the smoothness of the Hamiltonian and the wave functions, the coupling  $V_{d\epsilon}(R)$  decays exponentially with energy and is therefore easily extrapolated. In a real system, the presence of, e.g., Coulomb cusps can lead to a different rate of decay. In the case of the NO-like model, it was sufficient to precalculate  $F(\epsilon, R)$  only to 10 a.u. for all

choices of the discrete state and then extrapolate up to 200 a.u.

The shape of the lower-energy peaks, on the other hand, is influenced by the discretization step of the energy grid  $\Delta E$ , as illustrated in Fig. 3(b). In this case, the issue is the insufficient sampling of  $\Gamma(\epsilon, R)$  at low energies, as it changes rapidly up to approximately 0.025 a.u. (approximately 0.7 eV). This inaccuracy can be removed using a better interpolation method or, ideally, a better sampling.

For all subsequent cross sections, we show converged results obtained with the optimal parameters of the energy grid for evaluation of the Hilbert transform.

### B. Testing a different approach to NRM construction using $F(\epsilon, R)$

To test the construction of the nonlocal models from the fixed-nuclei level-shift function  $F(\epsilon, R)$  calculated as in Eq. (44), we use various definitions of the discrete states as described in Sec. III A and apply the procedure described in Sec. III B to obtain nonlocal models for all three two-dimensional models ( $N_2$ , NO, and  $O_2$ ) specified in Sec. II A. The resulting cross sections are then compared with the exact ones obtained by the numerical solution of the full 2D models and also with the cross sections determined within the nonlocal models constructed directly from the matrix elements (16) and (17) including the complex phase.

As shown in [28] and also in the results below, the NRM based on the constant discrete state gives almost perfect results for inelastic processes for  $N_2$ -like and NO-like models, but there is a significant background contribution in the elastic

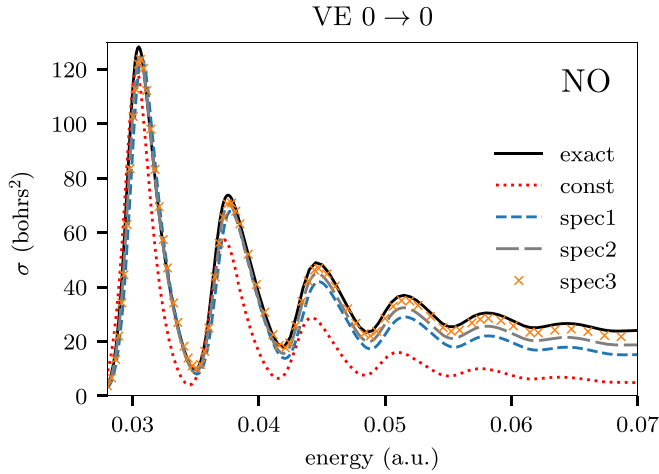


FIG. 7. Dependence of the elastic cross section on the choice of discrete state, compared with the exact cross section calculated from the NO-like two-dimensional model.

cross sections. These background contributions can be almost eliminated by choosing more-compact  $R$ -dependent discrete states such as the special discrete states described in Sec. III A (see [28] for more details where this effect is shown for the  $F_2$ -like model).

Here we demonstrate the elimination of the background contribution in the case of the NO-like and  $O_2$ -like models, for which we construct three and two special discrete states, respectively, each differing in the value of  $\lambda_{-\infty}$ , making them more and more compact. The parameters  $c$  and  $R_d$  are kept constant and chosen in such a way as to provide a smooth transition of all chosen compact discrete states at small internuclear distances to the electronic bound state in the limit  $R \rightarrow \infty$ .

Figure 4 shows the potential energy curves for the NO-like model with the corresponding discrete-state potentials  $V_d(R)$ . The parameters defining the discrete states are  $\lambda_{-\infty} = 8$  (denoted by spec1),  $\lambda_{-\infty} = 10$  (denoted by spec2), and  $\lambda_{-\infty} = 15$  (denoted by spec3), with common values  $c = 1.8$  and  $R_d = 3.0$ . Although the discrete-state potentials  $V_d(R)$  and also corresponding fixed-nuclei resonance widths  $\Gamma(\varepsilon, R)$  and level-shift functions  $\Delta(\varepsilon, R)$  shown in Fig. 5 differ rather significantly, the changes in the inelastic cross sections are negligible, as one can observe in Fig. 6, where the vibrational excitation (VE) cross sections for transition  $0 \rightarrow 1$  are shown for the constant and three special discrete states. The only significant discrepancies can be observed in the elastic cross sections at higher energies as shown in Fig. 7.

It is important to realize that the correct energy dependence of the cross sections (positions and shapes of peaks) is given mostly by the shape of the potential energy curve  $V_{\text{ion}}(R)$ , which is properly reproduced here within each nonlocal resonance model. As the potential  $V_d(R)$  moves away from  $V_{\text{ion}}(R)$  for different choices of the special discrete states,  $\Gamma(\varepsilon, R)$  and  $\Delta(\varepsilon, R)$  increase (as one can see in Fig. 5), resulting in the correct position of the effective local potential  $V_{\text{ion}}(R)$  within the nonlocal models. This shows that in principle one can almost fully encompass the background contribution into the

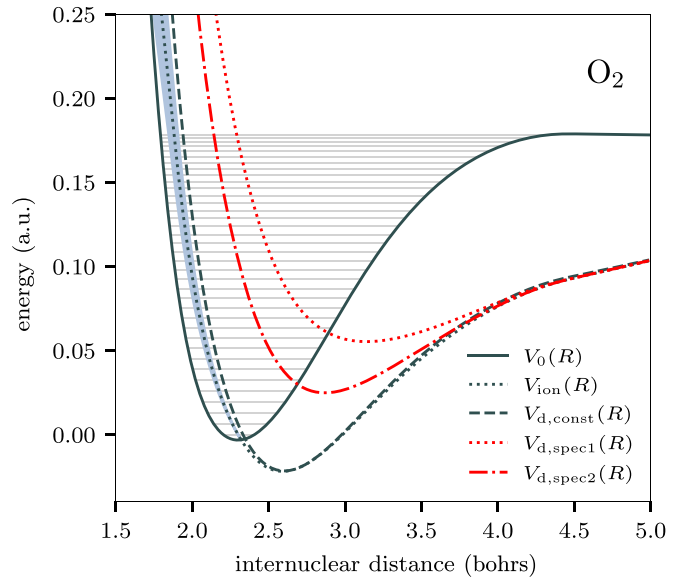


FIG. 8. Potential energy curves of the  $O_2$ -like model: the neutral potential  $V_0(R)$ , the negative ion resonance  $V_{\text{ion}}(R)$ , and the resonance width (shown by the shaded area) together with the discrete-state potential  $V_d(R)$  for the constant and the special choices of the discrete state.

nonlocal model by selecting a suitable discrete state, but as shown above in Sec. IV A, at a higher computational cost as  $\Gamma(\varepsilon, R)$  is much larger at higher energies for the special discrete states than for the constant discrete state.

The same calculations were performed for the  $O_2$ -like model, with the special discrete state 1 given by  $\lambda_{-\infty} = 8$ ,  $c = 1.8$ , and  $R_d = 3.0$  and special discrete state 2 by  $\lambda_{-\infty} = 3.29$ ,  $c = 1.8$ , and  $R_d = 3.0$ . The potential energy curves are shown in Fig. 8 and cross sections for the elastic channel are shown in Fig. 9. However, it is not in general true that a more-compact discrete state yields better cross sections. In this case, special discrete state 1 overestimates the background contribution.

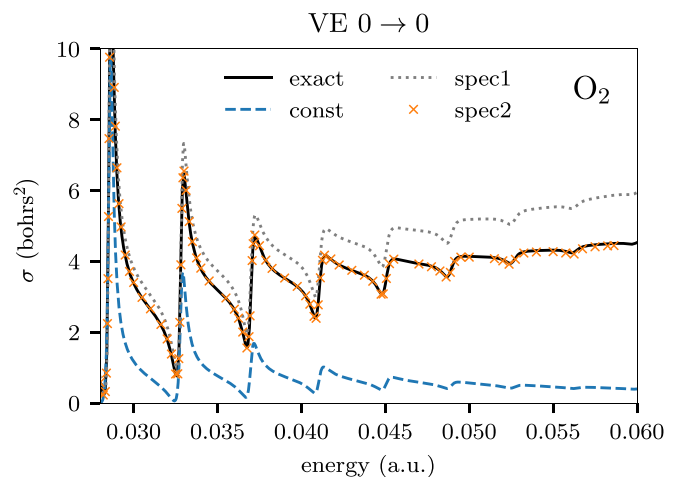


FIG. 9. Dependence of the elastic cross section on the choice of discrete state, compared with the exact cross section calculated from the  $O_2$ -like two-dimensional model.

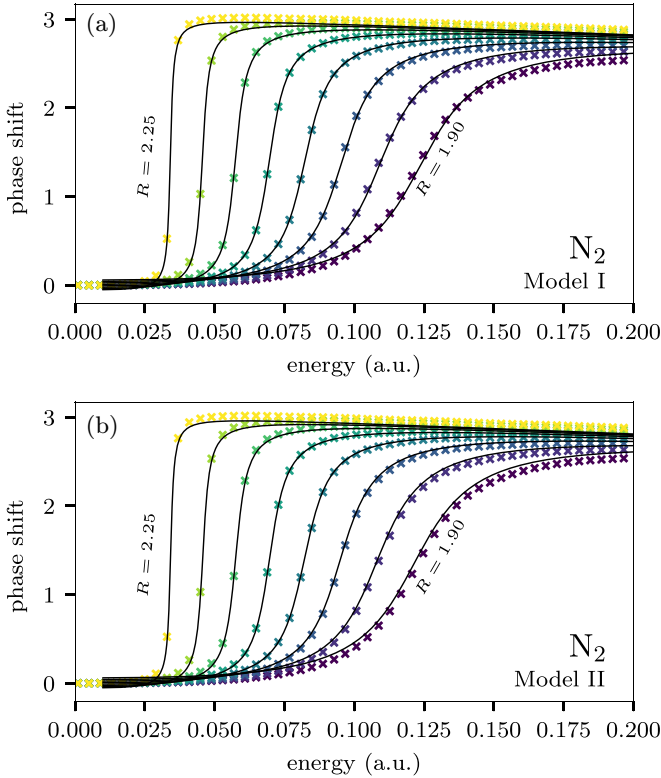


FIG. 10. Fitted phase shifts from (a) model I (lines) and (b) model II (lines) compared to fixed-nuclei scattering phase shifts from the  $N_2$ -like model (points). Curves from right to left correspond to internuclear distances of 1.90, 1.95, 2.00, 2.05, 2.10, 2.15, 2.20, and 2.25 a.u.

TABLE IV. Parameters of the fitted model I for  $N_2$  for functions in (50). We omitted superscripts for simplicity as there is just one term in  $V_{d\varepsilon}(R)$  in this model. All values are in atomic units.

Parameter	Value	Parameter	Value
$n$	1	$E_{EA}$	0.243217
$D_d$	0.42791	$a_0$	-2.22208
$\alpha_d$	1.17203	$a_1$	6.88415
$R_d$	2.20015	$a_2$	0.14138
$b_0$	1.19712	$b_1$	3.56770
$c_0$	-1.20402	$c_1$	-0.07258

TABLE V. Same as in Table IV but for model II for  $N_2$ .

Parameter	Value	Parameter	Value
$n$	1	$E_{EA}$	0.243216
$a_0$	0.0	$b_0$	1.07703
$a_1$	1.82533	$b_1$	0.0
$a_2$	0.17952		
$c_0$	-1.26202	$c_1$	-0.07290

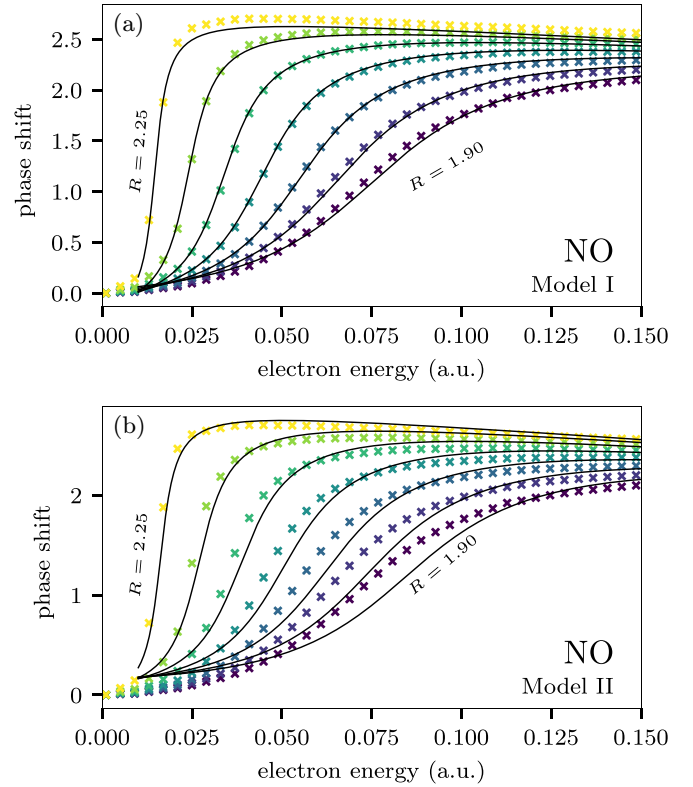


FIG. 11. Fitted phase shifts from (a) model I (lines) and (b) model II (lines) compared to fixed-nuclei scattering phase shifts from the NO-like model (points). Curves from right to left correspond to internuclear distances of 1.90, 1.95, 2.00, 2.05, 2.10, 2.15, 2.20, and 2.25 a.u.

Except for the background contribution, there is practically no discrepancy between the cross sections calculated directly from the complex coupling  $V_{d\varepsilon}(R)$  and the cross sections calculated from the *ab initio* level-shift function  $F(\varepsilon, R)$ . Let us recall that the two methods differ only in neglecting the complex phase of  $V_{d\varepsilon}(R)$  in the latter method. The complete overview of the results is given in the Supplemental Material [36], where the cross sections together with the potential energy curves and  $\Gamma(\varepsilon, R)$ ,  $\Delta(\varepsilon, R)$ , and  $\phi_d(r; R)$  for selected energies and internuclear distances are plotted for all 2D models and chosen discrete states.

### C. Fitting nonlocal resonance models to scattering phase shifts

For comparison with the approach introduced above, we also constructed several nonlocal resonance models through the traditional approach, i.e., fitting to known scattering data, in our case fixed-nuclei phase shifts obtained by solving the one-dimensional scattering problem resulting from fixing  $R$  within the two-dimensional models. We define two kinds of nonlocal resonance models I and II which differ in the way the discrete-state potential is obtained. Model I assumes the dependence of potentials, coupling, and background phase

TABLE VI. Parameters of the fitted model I for NO for functions in (50). All values are in atomic units.

Parameter	Value	Parameter	Value
$n$	2	$E_{EA}$	0.059710
$D_d$	0.15600	$\alpha_d$	1.19874
$R_d$	2.48595		
$a_0^1$	-3.52449	$a_0^2$	-0.54670
$a_1^1$	2.13657	$a_1^2$	2.84100
$a_2^1$	1.93383	$a_2^2$	0.32056
$b_0^1$	$1.96172 \times 10^{-4}$	$b_0^2$	$0.32618 \times 10^{-4}$
$b_1^1$	7.55701	$b_1^2$	3.63948
$c_0$	-1.85637	$c_1$	-0.34785

shift on internuclear distance and energy

$$\begin{aligned}
 V_0(R) &= D_0(1 - e^{\alpha_0(R-R_0)})^2 - D_0 + E_{EA}, \\
 V_d(R) &= D_d(1 - e^{\alpha_d(R-R_d)})^2 - D_d, \\
 V_{d\varepsilon}(R) &= \varepsilon^\alpha \sum_{i=1}^n A_i(R) e^{-B_i(R)\varepsilon}, \\
 A_i(R) &= (a_0^i R + a_1^i) e^{-a_2^i R}, \\
 B_i(R) &= b_0^i R + b_1^i, \\
 \delta_{bg}(\varepsilon) &= c_0 \varepsilon + c_1,
 \end{aligned} \tag{50}$$

where the discrete-state potential  $V_d(R)$  is fixed as a Morse potential. In contrast, model II does not assume any particular form of the discrete-state potential since it is reconstructed from the known resonance energy following Eq. (48). The latter approach has already been successfully used to construct a nonlocal resonance model for the  $O_2$  molecule in [31] and can be applied only in the case where a clear resonance appears. Here we demonstrate that this approach can also be used for the  $N_2$ -like and NO-like two-dimensional models.

The fits to obtain the unknown parameters of the models were performed using the Nelder-Mead algorithm [37] minimizing the mean-square error. The resulting fitted phase shifts compared with exact phase shifts calculated within the two-dimensional models are shown in Fig. 10 for  $N_2$  and in Fig. 11 for NO. The obtained parameters of the models are listed in Tables IV–VII.

Figures 12 and 13 show the potential energy curves of the  $N_2$ -like and NO-like models together with the discrete-state potential  $V_d(R)$  of the fitted nonlocal resonance models. For comparison, we also show  $V_d(R)$  corresponding to the constant choice of the discrete state.

TABLE VII. Same as in Table IV but for model II for NO.

Parameter	Value	Parameter	Value
$n$	1	$E_{EA}$	0.059710
$a_0$	4.81029	$b_0$	0.10444
$a_1$	0.99923	$b_1$	5.03081
$a_2$	1.23990		
$c_0$	-2.59928	$c_1$	-0.17042

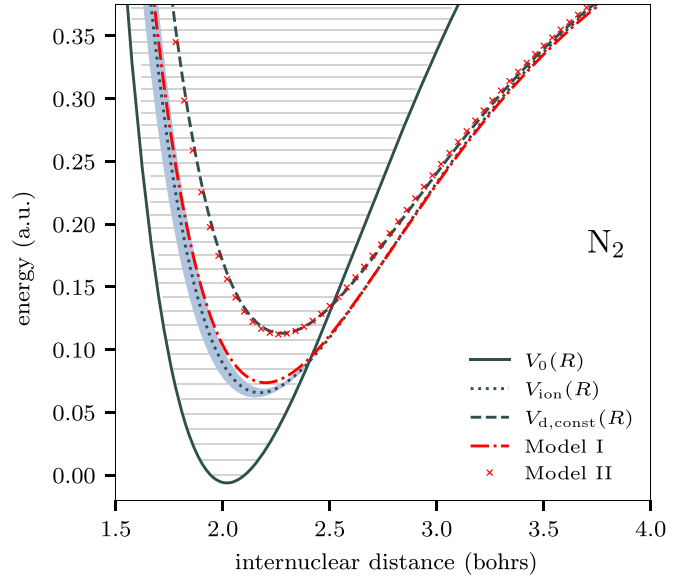


FIG. 12. Potential energy curves of the  $N_2$ -like model: the neutral potential  $V_0(R)$ , the negative ion resonance  $V_{ion}(R)$ , and the resonance width (shown by the shaded area). The discrete-state potential  $V_d(R)$  corresponding to the constant choice of the discrete state is compared with  $V_d(R)$  coming from the two fitted models I and II.

stant choice of the discrete state. The Morse potential chosen for model I is not very flexible and often fails to be close to the ion potential curve  $V_{ion}(R)$ , as in the case of NO. On the other hand,  $V_d(R)$  reconstructed from  $V_{ion}(R)$  tends to follow the constant discrete-state potential closely.

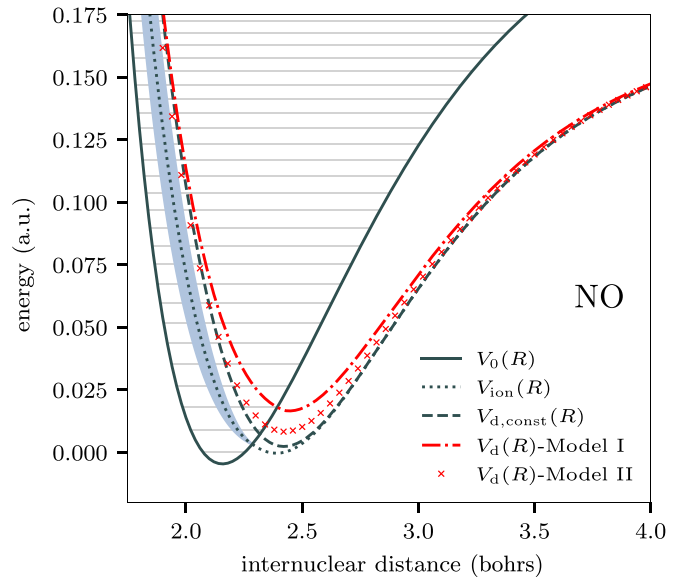


FIG. 13. Potential energy curves of the NO-like model: the neutral potential  $V_0(R)$ , the negative ion resonance  $V_{ion}(R)$ , and the resonance width (shown by the shaded area). The discrete-state potential  $V_d(R)$  corresponding to the constant choice of the discrete state is compared with  $V_d(R)$  coming from the two fitted models I and II.

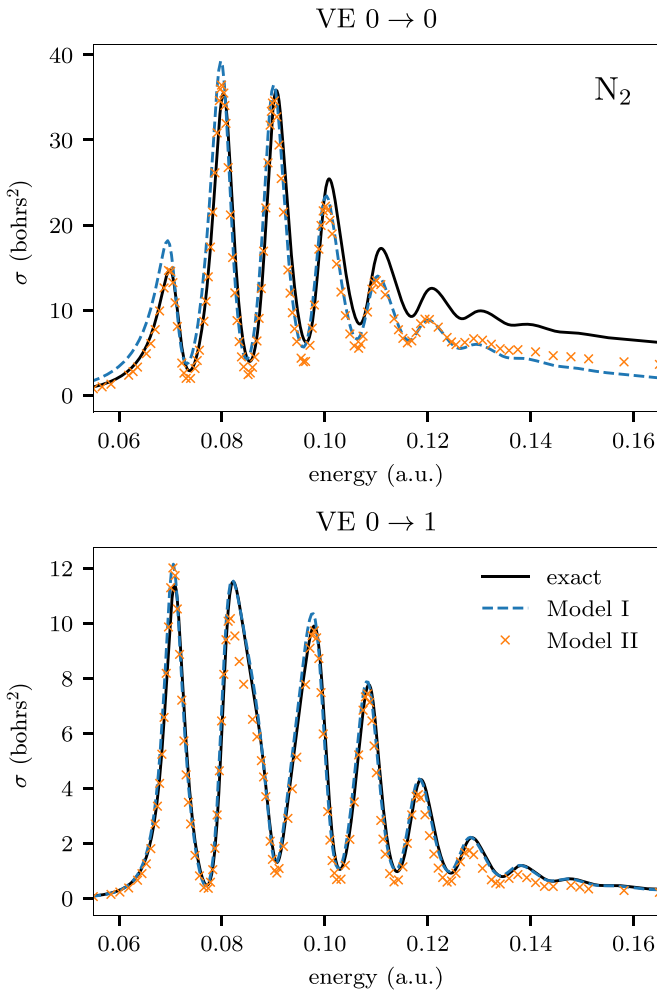


FIG. 14. Exact vibrational excitation cross sections from the  $N_2$ -like two-dimensional model compared with the results from the two nonlocal resonant models described by Eqs. (50) and fitted to the fixed-nuclei scattering phase shifts.

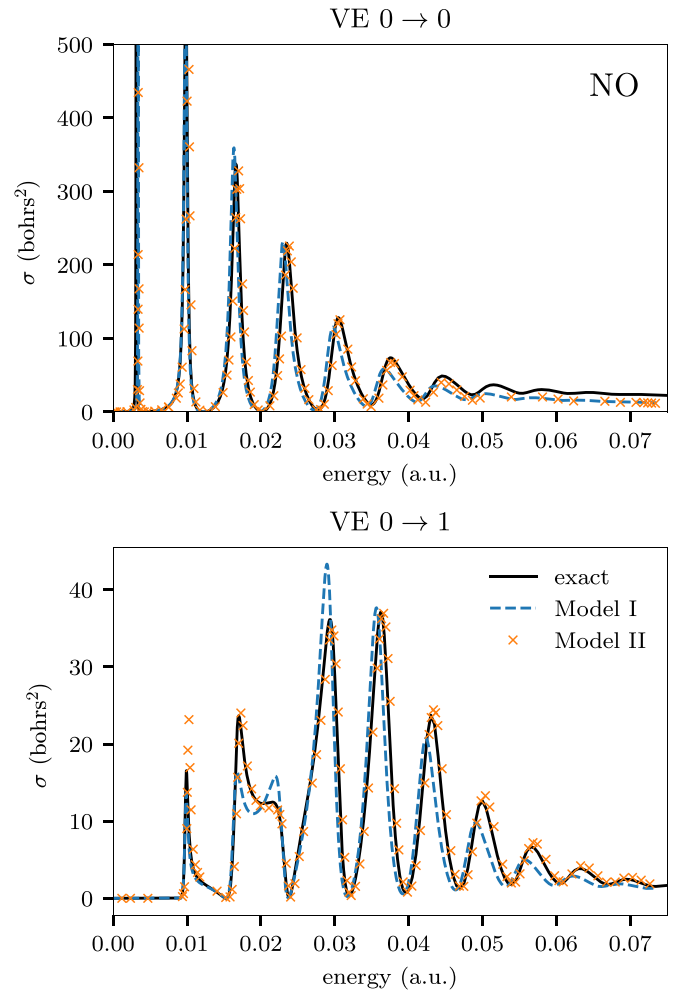


FIG. 15. Exact vibrational excitation cross sections from the  $NO$ -like two-dimensional model compared with the results from the two nonlocal resonant models described by Eqs. (50) and fitted to the fixed-nuclei scattering phase shifts.

The cross sections obtained for the fitted models I and II are compared with the exact results from the two-dimensional model in Fig. 14 for  $N_2$  and in Fig. 15 for  $NO$ . In the case of  $N_2$ , the most significant difference between the two models is in the background contribution in the elastic channel; otherwise, the agreement is good, although the results in the inelastic channels are slightly better for model I than for model II.

In the  $NO$  case,  $V_{ion}(R)$  coming from model I agreed with the exact  $V_{ion}(R)$  only in the inner region (because of the good agreement of the phase shifts), but not in the outer region. This is because the Morse potential used as  $V_d(R)$  does not match the long-range behavior of the negative ion. Therefore, we modified  $V_d(R)$  in the outer region by adding a correction  $\Delta V_{ion}(R)$  calculated as the difference between  $V_{ion}(R)$  from model I and the exact  $V_{ion}(R)$  from the two-dimensional model. This is well justified because in the outer region, i.e., where the extra electron is bound, the  $V_{ion}(R)$  curve is generally known, e.g., from quantum chemistry calculations. The final corrected discrete-state energy curve  $V_d^{corr}(R)$  curve of

model I is given by

$$V_d^{corr}(R) = V_d(R) + \Delta V_{ion}(R). \quad (51)$$

Even though both models I and II give the correct negative-ion curve  $V_{ion}(R)$ , there are some notable discrepancies. In Fig. 11 we see that model I reaches much better agreement of the fixed-nuclei scattering phase shifts than model II; however, model II gives cross sections that have better agreement with the exact results (apart from the background contribution in the elastic channel).

The fitting procedure for model II is also easier because there are fewer parameters to fit since the discrete-state potential  $V_d(R)$  is reconstructed directly and no functional form is assumed. Thus in this approach we get the correct behavior of  $V_d(R)$  consistent with the dynamics of the collisional complex for large internuclear distances  $R$ . Choosing a fixed functional form of  $V_d(R)$  seems to be too restrictive and makes the fitting tedious and unreliable.

The phase shifts in Figs. 10 and 11 however show that one cannot always tell from the quality of the fit how well the

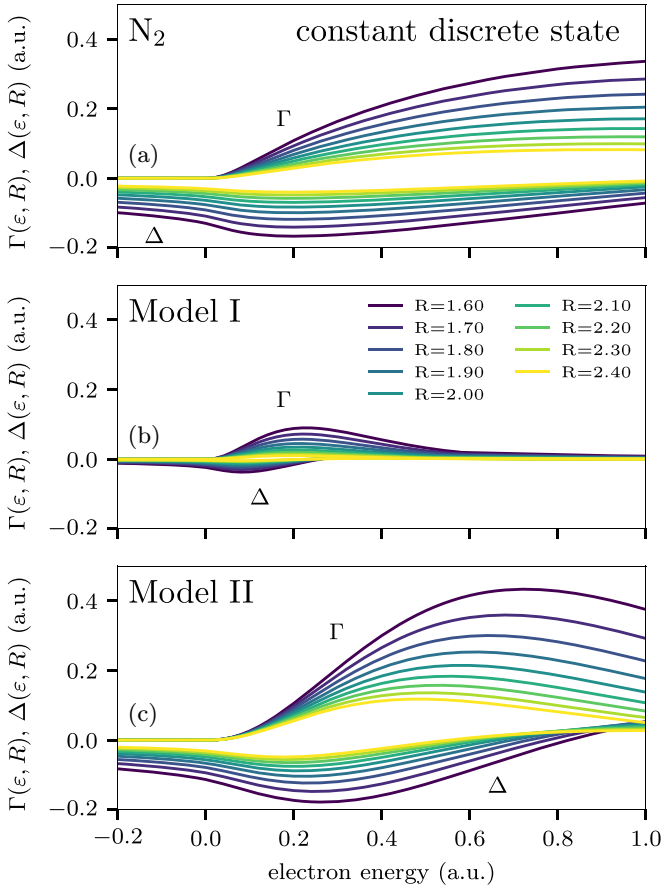


FIG. 16. Fixed-nuclei level-shift functions  $\Delta(\epsilon, R)$  and resonance widths  $\Gamma(\epsilon, R)$  coming from (b) and (c) two different fits with (a) the exact form for several internuclear distances.

resulting model would perform. Model II for NO gives the worst agreement with the scattering phase shifts but produces flawless cross sections. Without the reference to the exact results (which one usually does not have at hand), such a model would probably get rejected during the fitting procedure.

Moreover, while both models for N<sub>2</sub> seem to work fine, their respective  $\Delta(\epsilon, R)$  and  $\Gamma(\epsilon, R)$  functions can differ greatly, as shown in Fig. 16. The situation is similar to the case of NO (see Fig. 17).

The reconstruction of  $V_d(R)$  from the known resonance energy generally leads to better results. While the bound part of the negative-ion potential-energy curve can be usually obtained using standard quantum chemistry packages, the complex part of the curve (usually given by resonance energy and width) is often unknown. Since  $V_d(R)$  should coincide with  $V_{\text{ion}}(R)$  outside the interaction region, one can use it to construct  $V_d(R)$  with the correct asymptotic behavior.

## V. CONCLUSION

In this work we proposed an alternative way of constructing nonlocal resonance models used to describe the nuclear dynamics of electron-molecule collisions. The method is based on the fact that the magnitude of the discrete-state-continuum coupling  $V_{d\epsilon}(R)$  can be calculated from the

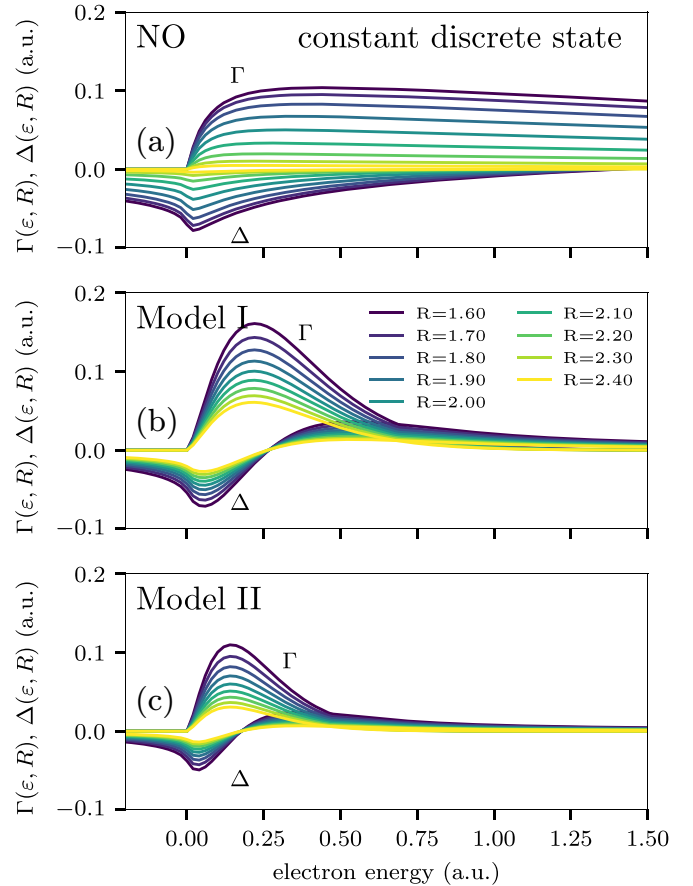


FIG. 17. Fixed-nuclei level-shift functions  $\Delta(\epsilon, R)$  and resonance widths  $\Gamma(\epsilon, R)$  coming from (b) and (c) two different fits with (a) the exact form for several internuclear distances.

fixed-nuclei *ab initio* level-shift function  $F(\epsilon, R)$  constructed by the projection of the full fixed-nuclei wave function on the preselected discrete state. This can be then used to construct the full nonlocal potential  $F(\epsilon, R, R')$  governing the nuclear dynamics within the discrete-state-in-continuum framework. The extension of the imaginary part of the fixed-nuclei level-shift function  $F(\epsilon, R)$  into the full nonlocal potential  $F(\epsilon, R, R')$  is straightforward if we neglect the phase of  $V_{d\epsilon}(R)$ . The Hilbert transform connecting the real and imaginary parts of the nonlocal potential  $F(E, R, R')$  has to be evaluated numerically. The assumption that neglecting the phase has little influence on the resulting dynamics was tested by comparison with the direct construction of  $V_{d\epsilon}(R)$  using the projection-operator formalism. We used a two-dimensional model [29] approximating the behavior of N<sub>2</sub>, NO, and O<sub>2</sub> molecules to test the proposed approach by comparing it to the numerically exact solution of the vibrational dynamics available for these models. We also compared it to results obtained with previously used NRM construction based on fitting of fixed-nuclei phase shifts.

The models built directly from  $V_{d\epsilon}(R)$  and from the *ab initio* level-shift function  $F(\epsilon, R)$  were constructed for all three two-dimensional models. In all cases, the agreement with the referential exact results was excellent. Moreover, we demonstrated that the choice of the discrete state  $\phi_d$ , being the

only remaining degree of freedom, regulates the contribution of background scattering in the elastic cross section while the inelastic cross sections practically do not change. However, there are computational complications in the evaluation of nonlocal potential  $F(\varepsilon, R, R')$  arising from certain choices of the discrete state. This was discussed in detail in the case of NO, but the same effect was observed also for  $N_2$  and  $O_2$ .

The comparison with the models constructed by fitting the fixed-nuclei scattering phase shifts was done for  $N_2$ -like and NO-like two-dimensional models. Since the fitting procedure is not unique, two models were constructed in each case. The results obtained using these nonlocal models showed the common shortcomings of this approach, which stem from the fact that there is no guarantee that a good fit of the fixed-nuclei data leads to an accurate description of the nuclear dynamics. Comparing two slightly different models constructed to reproduce the fixed-nuclei phase shifts, we observed that the model with a seemingly better fit can give slightly worse results for vibrational excitation cross

sections than the model with a seemingly worse fit of phase shifts. Another limitation of the fitting procedure stems from the fixed functional form of the model.

On the other hand, the downside of our alternative method of constructing the nonlocal models is the need to evaluate the coupling  $V_{de}(R)$  to high energies, which may be difficult or impossible for real systems. This can be partially circumvented by extrapolation, as shown for the NO-like model. We believe that this approach can be applied to real systems since the evaluation of the level-shift function  $F(\varepsilon, R)$  using Eq. (44) can be straightforwardly implemented, e.g., in the UKRmol+  $R$ -matrix codes [38] and that this will be an important simplification as compared to the fitting approach, especially for polyatomic molecules.

#### ACKNOWLEDGMENTS

The study was supported by Charles University Grant Agency Project No. 552120 (V.A.), and by the Czech Science Foundation Project No. 24-11166S (M.Č. and K.H.).

- 
- [1] G. J. Schulz, Resonances in electron impact on diatomic molecules, *Rev. Mod. Phys.* **45**, 423 (1973).
- [2] *Low-Energy Electron Scattering from Molecules, Biomolecules and Surfaces*, edited by P. Čársky and R. Čurík (CRC, Boca Raton, 2012).
- [3] *Computational Methods for Electron-Molecule Collisions*, edited by W. M. Huo and F. A. Gianturco (Plenum, New York, 1995).
- [4] D. T. Birtwistle and A. Herzenberg, Vibrational excitation of  $N_2$  by resonance scattering of electrons, *J. Phys. B* **4**, 53 (1971).
- [5] W. Domcke, Theory of resonance and threshold effects in electron-molecule collisions: The projection-operator approach, *Phys. Rep.* **208**, 97 (1991).
- [6] B. I. Schneider, M. Le Dourneuf, and P. G. Burke, Theory of vibrational excitation and dissociative attachment: An  $R$ -matrix approach, *J. Phys. B* **12**, L365 (1979).
- [7] C. Mündel and W. Domcke, Nuclear dynamics in resonant electron-molecule scattering beyond the local approximation: model calculations on dissociative attachment and vibrational excitation, *J. Phys. B* **17**, 3593 (1984).
- [8] M. Berman, H. Estrada, L. S. Cederbaum, and W. Domcke, Nuclear dynamics in resonant electron-molecule scattering beyond the local approximation: The 2.3-eV shape resonance in  $N_2$ , *Phys. Rev. A* **28**, 1363 (1983).
- [9] H. Feshbach, Unified theory of nuclear reactions, *Ann. Phys. (NY)* **5**, 357 (1958).
- [10] H. Feshbach, A unified theory of nuclear reactions. II, *Ann. Phys. (NY)* **19**, 287 (1962).
- [11] J. C. Y. Chen, Dissociative attachment in rearrangement electron collision with molecules, *Phys. Rev.* **148**, 66 (1966).
- [12] T. F. O'Malley, Theory of dissociative attachment, *Phys. Rev.* **150**, 14 (1966).
- [13] J. N. Bardsley, Configuration interaction in the continuum states of molecules, *J. Phys. B* **1**, 349 (1968).
- [14] W. Domcke and L. S. Cederbaum, A simple formula for the vibrational structure of resonances in electron-molecule scattering, *J. Phys. B* **10**, L47 (1977).
- [15] W. Domcke, L. S. Cederbaum, and F. Kaspar, Threshold phenomena in electron-molecule scattering: a non-adiabatic theory, *J. Phys. B* **12**, L359 (1979).
- [16] L. S. Cederbaum and W. Domcke, Local against non-local complex potential in resonant electron-molecule scattering, *J. Phys. B* **14**, 4665 (1981).
- [17] K. Houfek and M. Čížek, in *Low-Energy Electron Scattering from Molecules, Biomolecules and Surfaces* (Ref. [2]), pp. 127–160.
- [18] R. S. Wilde, G. A. Gallup, and I. I. Fabrikant, Comparative studies of dissociative electron attachment to methyl halides, *J. Phys. B* **33**, 5479 (2000).
- [19] M. Zawadzki, M. Čížek, K. Houfek, R. Čurík, M. Ferus, S. Civiš, J. Kočíšek, and J. Fedor, Resonances and dissociative electron attachment in HNCO, *Phys. Rev. Lett.* **121**, 143402 (2018).
- [20] H. B. Ambalampitiya and I. I. Fabrikant, Nonlocal complex potential theory of dissociative electron attachment: Inclusion of two vibrational modes, *Phys. Rev. A* **102**, 022802 (2020).
- [21] I. I. Fabrikant, Quasiclassical  $R$ -matrix theory of inelastic processes in collisions of electrons with HCl molecules, *Phys. Rev. A* **43**, 3478 (1991).
- [22] Some of these calculations are performed within the single-pole  $R$ -matrix approximation, which has been shown to be dynamically equivalent to the NRM [21].
- [23] J. Dvořák, M. Ranković, K. Houfek, P. Nag, R. Čurík, J. Fedor, and M. Čížek, Vibronic coupling through the continuum in the  $e + CO_2$  system, *Phys. Rev. Lett.* **129**, 013401 (2022).
- [24] J. Dvořák, K. Houfek, and M. Čížek, Vibrational excitation in the  $e + CO_2$  system: Nonlocal model of  $\Sigma\Pi$  vibronic coupling through the continuum, *Phys. Rev. A* **105**, 062821 (2022).
- [25] J. Dvořák, M. Ranković, K. Houfek, P. Nag, R. Čurík, J. Fedor, and M. Čížek, Vibrational excitation in the  $e + CO_2$  system: Analysis of the two-dimensional energy-loss spectrum, *Phys. Rev. A* **106**, 062807 (2022).

- [26] M. Berman, C. Mündel, and W. Domcke, Projection-operator calculations for molecular shape resonances: The  $^2\Sigma_u^+$  resonance in electron-hydrogen scattering, *Phys. Rev. A* **31**, 641 (1985).
- [27] C. Mündel, M. Berman, and W. Domcke, Nuclear dynamics in resonant electron-molecule scattering beyond the local approximation: Vibrational excitation and dissociative attachment in  $H_2$  and  $D_2$ , *Phys. Rev. A* **32**, 181 (1985).
- [28] K. Houfek, T. N. Rescigno, and C. W. McCurdy, Probing the nonlocal approximation to resonant collisions of electrons with diatomic molecules, *Phys. Rev. A* **77**, 012710 (2008).
- [29] K. Houfek, T. N. Rescigno, and C. W. McCurdy, Numerically solvable model for resonant collisions of electrons with diatomic molecules, *Phys. Rev. A* **73**, 032721 (2006).
- [30] L. H. Scarlett, I. Bray, and D. V. Fursa, Electronic and vibrational close-coupling method for resonant electron-molecule scattering, *Phys. Rev. Lett.* **127**, 223401 (2021).
- [31] V. Alt and K. Houfek, Resonant collisions of electrons with  $O_2$  via the lowest-lying  $^2\Pi_g$  state of  $O_2^-$ , *Phys. Rev. A* **103**, 032829 (2021).
- [32] M. Čížek and K. Houfek, in *Low-Energy Electron Scattering from Molecules, Biomolecules and Surfaces* (Ref. [2]), pp. 91–126.
- [33] F. W. King, *Hilbert Transforms*, Encyclopedia of Mathematics and its Applications Ser. No. 124 (Cambridge University Press, Cambridge, 2009), Vol. 1.
- [34] *The Schur Complement and Its Applications*, edited by F. Zhang (Springer, New York, 2005).
- [35] T. N. Rescigno and C. W. McCurdy, Numerical grid methods for quantum-mechanical scattering problems, *Phys. Rev. A* **62**, 032706 (2000).
- [36] See Supplemental Material at <http://link.aps.org/supplemental/10.1103/PhysRevA.109.052817> for the potential energy curves and the cross sections.
- [37] J. A. Nelder and R. Mead, A simplex method for function minimization, *Comput. J.* **7**, 308 (1965).
- [38] Z. Mašín, J. Benda, J. D. Gorfinkiel, A. G. Harvey, and J. Tennyson, UKRmol+: A suite for modelling electronic processes in molecules interacting with electrons, positrons and photons using the R-matrix method, *Comput. Phys. Commun.* **249**, 107092 (2020).